Acta Pharmacologica Sinica

www.nature.com/aps

ARTICLE

Discovery of a novel DDRs kinase inhibitor XBLJ-13 for the treatment of idiopathic pulmonary fibrosis

Ying Dong[1,2], Bi-xi Tang[1,2,3], Qi Wang[2,4], Li-wei Zhou[4,5], Cong Li[1], Xuan Zhang[1,2], Dan-dan Sun[6], Xin Sun[7], Xue-mei Zhang[3], Bing Xiong[2,4], Jia Li[1,2,8,9], Hong Shi[10], Dan-qi Chen[4] and Yi Zang[1,2,9]

Idiopathic pulmonary fibrosis (IPF) is a chronic fatal lung disease characterized by destruction of lung parenchyma and deposition of extracellular matrix in interstitial and alveolar spaces. But known drugs for IPF are far from meeting clinical demands, validation of drug targets against pulmonary fibrosis is in urgent demand. Tyrosine kinase receptor DDRs has been considered as a potential therapeutic target for pulmonary fibrosis due to its pathological collagen binding property and the roles in regulating extracellular matrix remodeling. In this study we designed and synthesized a new indazole derivative XBLJ-13, and identified XBLJ-13 as a highly specific and potent DDRs inhibitor with anti-inflammation and anti-fibrosis activities. We first demonstrated that DDR1/2 was highly expressed in the lung tissues of IPF patients. Then we showed that XBLJ-13 potently inhibited DDR1 and DDR2 kinases with IC_{50} values of 17.18 nM and 15.13 nM, respectively. Among a panel of 34 kinases tested, XBLJ-13 displayed relatively high selectivity for DDRs with minimal inhibitory effect on PDGFR family and FGFR1, as well as Abl kinase that had high homology with DDRs. Extensive profiling of XBLJ-13 revealed that the new inhibitor had much lower toxicity than nintedanib and better pharmacokinetic properties in mice. Furthermore, pharmacodynamic evaluation conducted in bleomycin-induced pulmonary fibrosis mice showed that administration of XBLJ-13 (30, 60, 90 $mg{\cdot}kg^{-1}{\cdot}d^{-1}$, i.g.) for 12 days significantly and dose-dependently ameliorated lung inflammation and fibrosis. Together, this study confirms that DDRs kinase is a potential target for PF, Particularly, compound XBLJ-13 is a highly potent and specific DDRs inhibitor, along with good pharmacokinetics profiles, and preferable in vivo efficacy, suggesting that it is a potential candidate for the treatment of PF.

Keywords: idiopathic pulmonary fibrosis; DDRs; kinase inhibitor; indazole derivatives; XBLJ-13; nintedanib; bleomycin-induced pulmonary fibrosismouse model

Acta Pharmacologica Sinica (2022) 43:1769–1779; https://doi.org/10.1038/s41401-021-00808-z

INTRODUCTION

Idiopathic pulmonary fibrosis (IPF) is a persistent and progressive lung disease. With the advent of global aging, the incidence rate of IPF is increasing year by year [1]. IPF is life-threatening with a median survival ranging from 2.5 to 3.5 years after diagnosis, and its fatality rate exceeds that of multiple cancers [2]. Many novel therapeutics are intensively pursued for the treatment of IPF. While only two drugs pirfenidone (Esbriet) and nintedanib (Ofev) have been approved by FDA for this devastating lung disease, which are still far from reversing the disease progression [3].

The pathogenesis of IPF is identified as a primarily fibrotic process characterized by the injured epithelial cells and abnormal wound healing involving epithelial mesenchymal transition (EMT), myofibroblast differentiation and exaggerated deposition of extracellular matrix (ECM) [4]. Among these, activated fibroblasts are termed as the chief criminal accumulating in the fibrotic tissues, which exacerbates deposition of ECM components, thus causing lung fibrosis and irreversible disruption of tissue architecture. In addition, the alveolar injury can cause subsequent macrophage polarization which accelerates tissue fibrosis [5].

Receptor tyrosine kinases (RTKs) are among the well appreciated therapeutic targets for fibrotic diseases [6]. The endogenous ligands activating these receptors are commonly growth factors or cytokines, with one noticeable exception—the discoidin domain receptors (DDRs) family including DDR1 and DDR2. DDR1 is primarily expressed in epithelial cells and mainly activated by collagens I–IV and VIII, while DDR2 is abundantly expressed in mesenchymal cells such as fibroblasts and only responds to fibrillar collagens, particularly collagen type I. Recently, collective evidence demonstrates that DDRs are critical mediators of lung

[1]State Key Laboratory of Drug Research, Shanghai Institute of Materia Medica, Chinese Academy of Sciences, Shanghai 201203, China; [2]University of Chinese Academy of Sciences, Beijing 100049, China; [3]Department of Pharmacology, School of Pharmacy, Fudan University, Shanghai 201203, China; [4]Department of Medicinal Chemistry, Shanghai Institute of Materia Medica, Chinese Academy of Sciences, Shanghai 201203, China; [5]Center for Supramolecular Chemistry and Catalysis and Department of Chemistry, College of Sciences, Shanghai University, Shanghai 200444, China; [6]School of Chinese Materia Medica, Nanjing University of Chinese Medicine, Nanjing 210023, China; [7]School of Pharmacy, Henan University, Kaifeng 475004, China; [8]Open Studio for Druggability Research of Marine Natural Products, Pilot National Laboratory for Marine Science and Technology (Qingdao), Qingdao 266237, China; [9]School of Pharmaceutical Science and Technology, Hangzhou Institute for Advanced Study, UCAS, Hangzhou 310024, China and [10]Department of Anesthesiology of Shanghai Pulmonary Hospital, School of medicine, Tongji University, Shanghai 200433, China
Correspondence: Hong Shi (ada-shi@139.com) or Dan-qi Chen (dqchen@simm.ac.cn) or Yi Zang (Yzang@simm.ac.cn)
These authors contributed equally: Ying Dong, Bi-xi Tang

Received: 12 April 2021 Accepted: 28 October 2021
Published online: 24 November 2021

fibrosis. DDR1 and DDR2 display distinct cellular distributions and functions. DDR1-deficiency mice showed a blunted phenotype of chemokine secretion and a resistance to fibrosis in response to bleomycin [7]. A similar situation was also found in LPS-induced organ injury [8]. Collagen-induced activation of DDR1 prominently amplifies the production of monocyte chemoattractant protein 1 and nitric oxide by macrophages during inflammatory responses [9]. As for DDR2, it mainly participates in TGF-β triggered activation of lung fibroblasts [10]. Activation of DDR2 was reported to increase the production of cytokines such as tumor-necrosis factor α (TNF-α) by human dendritic cells, which is an important inflammatory factor to aggravate fibrosis [11]. The activation of DDR2 by collagen I was also shown to induce the expression of DDR1 in human lung fibroblasts, indicating the potential crosstalk between the two receptors [12]. Therefore, dual inhibition of DDR1 and DDR2 might be a promising strategy for anti-fibrosis drug discovery.

In previous studies, some potent DDRs inhibitors have been reported, but most of these compounds showed less specific selectivity toward DDRs or the efficacy in lung fibrosis in vivo remains elusive. For instance, imatinib, nilotinib, and dasatinib also show strong inhibition of Abl, c-Kit in addition to DDRs [13]. VU6015929 exhibits strong DDR1 and DDR2 inhibitory activities, while it lacks animal data to prove its efficacy [14]. Together, these compounds have raised great interest in DDRs as an antifibrotic therapeutic target. However, either cytotoxicity, kinome selectivity, DMPK profiles or the in vivo efficacy of these inhibitors have not offer more definitive concept studies from being performed. Thus, it is highly desirable to identify new specific DDRs inhibitors for biological investigation and therapeutic development. Herein, we reported a potent and specific DDRs inhibitor, XBLJ-13, which could dose dependently inhibit lung fibroblast activation and alleviate the fibrosis progression in bleomycin-induced pulmonary fibrosis mice model with good pharmacokinetic properties. Our findings may pharmacologically promote the better understanding of the therapeutic target of DDRs in lung fibrosis and address the potential of XBLJ-13 to be a promising lead compound for further drug development against IPF.

MATERIALS AND METHODS

Compounds

The synthesis information of the compound is available in Supplementary information.

Lung tissues form IPF patient

Three human lung tissue samples (1.5 cm × 1.5 cm × 1.5 cm) were from Shanghai Pulmonary Hospital and were obtained from patients undergoing biopsy or transplantation. The normal part sections of patients with IPF have been used as normal controls. And the patients' detailed information was provided in the Supplementary information. The patients were pathologically confirmed as interstitial pneumonia with fibrosis at the Shanghai Pulmonary Hospital, China. Informed consent was obtained from the patients and this study was approved by the Chinese Clinical Trail Registry (ChiCTR1900028235).

Molecular modeling

The crystal structure 6GWR was selected for preparing for the 3D structure of DDR1 protein. And the 3D structure of DDR2 kinase domain (GenBank: AAH52998.1, aa. 557–851) was built by the online homology modeling server (https://swissmodel.expasy.org/), with the crystal structure of DDR1 (PDB ID: 6GWR) as the template. All the default parameters implemented in the server were adopted, and the statistics of final 3D model structure indicated the model structure is suitable for further docking study. Then, the DDR1 and DDR2 model structures were processed with protein preparation module in Schrödinger software package, and ATP binding site was selected for making the grid file with Glide module. Then the ligands were prepared to add the partial charge and minimize to obtain the low-energy conformation. Finally, ligands were docked into the grid files with default parameters at extra precision (XP) mode, and the predicted binding modes were depicted with Pymol software.

Cell culture

The MRC5, HEK293T and Beas-2B cell lines were purchased from ATCC. MRC5 fibroblast cells were cultured in Eagle's minimal essential medium (EMEM)(2176640, VWR Life Science, PA, USA) and HEK293T and Beas-2B cells were grown in Dulbecco's modified Eagle's medium (DMEM), both of which were supplemented with 10% fetal bovine serum (30–2003, Gibco, Waltham, MA, USA), 100 units/mL penicillin, and 100 μg/mL streptomycin at 37 °C in a 5% CO_2 humidified atmosphere. Cells were propagated at confluence by trypsinization.

Time-resolved fluorescence resonance energy transfer (TR-FRET) binding assay

IC_{50} against DDRs and ABL was determined by the Time-Resolved fluorescence resonance energy transfer (TR-FRET) binding assay as previously described [14]. Briefly, inhibitors at the different concentrations were incubated with Flag-tagged DDR1 or DDR2 cytoplasmic domain (1.25 nM), Eu-Anti-GST antibody (0.625 nM) and the kinase tracer 178 (6.25 nM for DDR1, or 1.25 nM for DDR2, Invitrogen) at room temperature for 2 h. With regard to ABL IC_{50} determination, ABL protein, peptide substrate and compounds of different concentrations were added to the 384 reaction plate. The final volume of the reaction is 10 μL (2%) DMSO, 0.002 ng/μL ABL, 1 μM TK peptide substrate, 30 μM ATP in HEPES buffer (50 mM HEPES, 5 mM $MgCl_2$, 2 mM DTT, 1 nM SEB), and incubated at room temperature for 0.5 h. Subsequently, the kinase reaction was quenched by the addition of Eu-labeled antibody and XL-665 in 1× Detection buffer containing 60 mM EDTA (Cisbio). The Fluorescence signal was collected on Envision with excitation at 320 nm and emission at 615 nm (donor) and 665 nm (acceptor). In the data processing, the ratio of the concentration to the active percentage was plotted, and then the fitting and curve were calculated using nonlinear regression.

ELISA kinase assay

The effects of indicated compound on the activities of various tyrosine kinases were determined using enzyme-linked immunosorbent assays (ELISAs) with purified recombinant proteins. Briefly, 20 μg/mL poly (Glu, Tyr) 4:1 (Sigma, St. Louis, MO, USA) was precoated in 96-well plates as a substrate. A 50-μL aliquot of 10 μM ATP solution diluted in kinase reaction buffer (50 mM HEPES [pH 7.4], 50 mM $MgCl_2$, 0.5 mM $MnCl_2$, 0.2 mM Na_3VO_4, and 1 mM DTT) was added to each well; 1 μL of indicated compound diluted in 1% DMSO (*v/v*) (Sigma, St. Louis, MO, USA) was then added to each reaction well. DMSO (1%, *v/v*) was used as the negative control. The kinase reaction was initiated by the addition of purified tyrosine kinase proteins diluted in 49 μL of kinase reaction buffer. After incubation for 60 min at 37 °C, the plate was washed three times with phosphate-buffered saline (PBS) containing 0.1% Tween 20 (PBST). Anti-phosphotyrosine (PY99) antibody (100 μL; 1:500, diluted in 5 mg/mL BSA T-PBS) was then added. After a 30-min incubation at 37 °C, the plate was washed three times, and 100 μL horseradish peroxidase-conjugated goat anti-mouse IgG (1:1000, diluted in 5 mg/mL BSA T-PBS) was added. The plate was then incubated at 37 °C for 30 min and washed 3 times. A 100-μL aliquot of a solution containing 0.03% H_2O_2 and 2 mg/mL *o*-phenylenediamine in 0.1 M citrate buffer (pH 5.5) was added. The reaction was terminated by the addition of 50 μL of 2 M H_2SO_4 as the color changed, and the plate was analyzed using a multiwell spectrophotometer (SpectraMAX190, Molecular Devices, Palo Alto, CA, USA) at 490 nm. The inhibition rate (%) was calculated

using the following equation: [1-(A_{490}/$A_{490\ control}$)] ×100%. The IC_{50} values were calculated from the inhibition curves in two separate experiments.

Cell viability assay
Cells were plated in 96-well plates and exposed to the indicated concentrations of XBLJ-13 (0.3125, 0.625, 1.25, 2.5, 5, 10, 20, 40 μM) or vehicle control (DMSO) for 72 h. Cell viability was examined with an CCK8 assay (D3100L4057, life ilab, Shanghai, China). CCK8 (10 μL) was added to each well and incubated for 1 h, after which the absorbance of the CCK8 signal was calculated after absorbance detection at 450 nm.

Western blot analysis
Western blot analyses were performed as described below. Briefly, cell lysates were prepared using lysis buffer and subjected to SDS-PAGE. After SDS-PAGE, PVDF membranes were probed with specific primary antibodies overnight: DDR1(5583, Cell Signaling Technology, Trask Lane Danvers, USA); DDR2 (12133, Cell Signaling Technology, Trask Lane Danvers, USA); Human Phospho-DDR1/DDR2 (Y796, Y740) Antibody (MAB25382, R&D,USA); GAPDH (ab8245, Abcam, Cambridge, UK); α-SMA (ab7817, Abcam, Cambridge, UK); Fibronectin (ab2413, Abcam, Cambridge, UK); collagen1-α1 (ab34710, Abcam, Cambridge, UK); SRC (2109, Cell Signaling Technology, Trask Lane Danvers, USA); Phospho-SRC (Tyr416) (59548, Cell Signaling Technology, Trask Lane Danvers, USA); Akt (pan) (4691, Cell Signaling Technology, Trask Lane Danvers, USA); Phospho-Akt (Ser473) (4060, Cell Signaling Technology, Trask Lane Danvers, USA); p44/42 MAPK (Erk1/2) (9194, Cell Signaling Technology, Trask Lane Danvers, USA); Phospho-p44/42 MAPK (Erk1/2) (Thr202/Tyr204) (8544, Cell Signaling Technology, Trask Lane Danvers, USA).

Real-time qPCR
Real-time qPCR was performed using the SYBR GREEN QPCR KIT (Q511–02, Vazyme, Nanjing, China) on Agilent Mx3000P as specified by the manufacturer. Total RNA was harvested from cells using TRIzol reagent (9109, TaKaRa, Dalian, China) and further purified using the standard protocol. The total RNA (1 μg) was transcribed into cDNA in 20 μL reactions using the prime script RT Master Mix (RR036B, TaKaRa, Dalian, China) and then diluted to 200 μL, which was used in subsequent real-time qPCR reactions. GAPDH was used as the normalization control. All reactions were performed in triplicates.

Wound healing assay
MRC5 were seeded at confluent status and the cell monolayer was scratched with a 10 μL pipette tip and washed twice with fresh medium. After treated with serum-free culture medium containing either DMSO or various concentrations of compounds for 48 h, the migratory area in the gap was measured using a light microscope at ×100 magnification.

Collagen gel contraction assay
The effects of XBLJ-13 on fibroblast-mediated gel contraction were determined in the presence or absence of TGF-β1(5 ng/mL, 10804-HNAC, Sino Biological Inc, Beijing, China) using a modification of the method developed by Peter Ngo et al. [15]. The collagen gel was prepared in 24-well plates. NaOH (0.1 mol/L) was used to adjust the pH and 10× PBS was used to adjust the solution to physiological strength. The mixed solution (500 μL) was added to each plate and incubated at 37 °C for 1 h to allow gelatinization. The floating gels were cultured for up to 2 days, and the ability of the fibroblasts to contact the gels was quantified daily using a ruler.

BLM-induced PF in mice
Male mice (C57BL/6), 8–10 weeks of age were purchased from SLAC and maintained in a 12 h light/dark cycle with free access to food and water. All experimental methods were carried out in accordance with the guidelines of the IACUC of Shanghai and the National Research Council Guide for the Care and Use of Laboratory Animals. All animal experiments were performed according to procedures approved by the Animal Care and Use Committee of the Shanghai Institute of Materia Medica. The male C57BL/6 mice (8 − 10 weeks) were randomly divided into six groups: control group, BLM group, XBLJ-13 treated group (30, 60, 90 mg/kg) and nintedanib-treated group (30 mg/kg). Each group was composed of eight mice. The animals received a single dose of BLM (BD01259671, Bidepharma, Shanghai, China) at 1.7 U/kg by intratracheal instillation or saline with MicroSprayer aerosolizer (BJ-PW-M, Bio Jane, Shanghai, China). Compounds XBLJ-13 and nintedanib were administered once daily through gavage for 12 days starting from the third day after the administration of bleomycin. BALF and lung tissue samples were collected at day 15 and mouse serum was collected for biochemical analysis.

Isolation and culture of murine lung fibroblasts
Murine lung fibroblasts were isolated using a method described previously. Briefly, mouse lungs were minced into 1–2 mm^3 pieces and incubated in calcium and magnesium free Hanks' balanced salt solution (HBSS) containing 0.3 mg/mL type IV collagenase (C5138, Sigma, Darmstadt, Germany) and 0.5 mg/mL trypsin for 60 min at 37 °C with shaking. The dissociated cells were centrifuged and cultured in FBS supplemented DMEM for 1 h, and then adherent fibroblasts were rinsed with HBSS and cultured in FBS supplemented DMEM. Mouse lung fibroblasts were used between passages 3 and 6.

Lung histology and imaging
Mouse lungs were inflated with 4 mL of 4% paraformaldehyde/PBS (PFA) solution embedded in paraffin. Sections (5-μm-thick, mouse) were deparaffinized in serial solutions of xylene and ethanol with decreasing concentration and water, followed by antigen retrieval by steaming in 10 mM citric acid (pH 6.0) for 20 min followed by a 20 min cooling period. The lung sections were washed with PBS buffer and blocked with 5% BSA for 60 min. Next, samples were incubated with anti-SMA antibody overnight at 4 °C and then rhodamin-labeled antibody for 60 min. The images were recorded by fluorescence microscope. We also processed paraffin embedded tissue sections for lung histology and immunohistochemical staining, including H&E and Masson's trichrome.

Hydroxyproline content of whole lung
Hydroxyproline content of whole lung was measured with Hydroxyproline Assay Kit according to the protocol (A030–2, Nanjing Jiancheng Bioengineering Institute, Nanjing, China). Briefly, mouse lung tissues were precisely weighed 30 mg to hydrolyze. Then we adjusted pH to neutrality and used activated charcoal to decolorize samples. Finally, the samples react with the corresponding detection solution and absorbance was measured (λ = 550 nm) using a BioTek ELx800 plate reader. The amount of hydroxyproline in samples was calculated using standard, prepared according to the manufacturer's protocol.

BALF analysis
The collected BALF was centrifuged at 1000 r/min for 10 min at 4 °C. The supernatant was used for protein concentration detection and subsequent cytokine determinations. The precipitation was resuspended using 50 μL of physiological saline. The total number of cells in the BALF was detected by a cell counting instrument.

Capture ELISA
HEK-293T cells expressing DDR1-FLAG or DDR2-FLAG were seeded in complete medium at 3×10^5 cells/well in 6 well plates. After 24 h, cells were serum-starved for 8 h, incubated with different concentrations of inhibitors for 30 min then treated with rat collagen I (10 μg/mL in 20 mM acetic acid). After 2 h, cells were

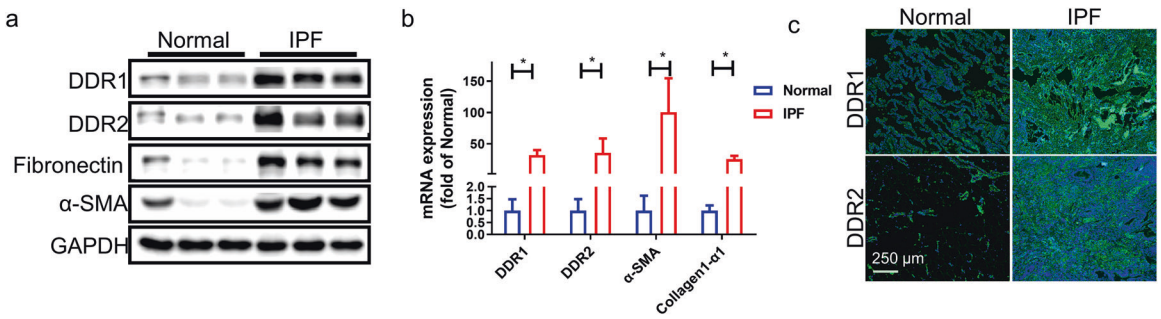

Fig. 1 DDR1 and DDR2 are concordantly highly expressed in fibrotic lungs. a, **b** The expression of DDR1 and DDR2 were highly expressed in fibrotic lung tissues compared with normal control in protein and mRNA levels. **c** Representative images of immunofluorescence staining of DDR1 (green) and DDR2 (green) of the IPF-diseased tissues (IPF) and the non-fibrosis region (Normal). The statistical significance was compared with the normal group using Student's *t* test analysis. $^{*}P < 0.05$.

washed with PBS and lysed in Cell Signaling Lysis Buffer supplemented with 1% Igepal, protease inhibitors and 2 mM sodium orthovanadate. Phosphorylated DDR1/2 and total DDR1/2 ELISA plates (DYC5859/C6170, R&D, Minneapolis, USA) were used to test with cell lysates (20 μg/well for detection of phosphorylated DDR1/2 or 4 μg/well for detection of total DDRs). The measurement was conducted according to the manufacture's instruction. The % DDR1 phosphorylation was determined using a calibration curve with samples treated with Collagen I in the absence of inhibitor (100% phosphorylation) or samples treated with 2 μM inhibitor without collagen I (0% phosphorylation). For curve fitting, comparison of fits and IC_{50} calculations we used GraphPad Prism software.

Mouse pharmacokinetics study

Compounds was dissolved in 1% Tween 80/water to a concentration of 1 mg/mL, and was given to ICR mice (SLAC, male, 18–22 g, $n = 3$) by gavage administration. Animal procedures were performed according to institutional ethical guidelines of animal care. Blood samples were collected at 0.25, 0.5, 1, 2, 4, 8, and 24 h after administration. Plasma 10 mL was added to solvent of methanol: acetonitrile (1:1, *v/v*) (100 mL) with internal standard and vortexed thoroughly. It was centrifuged for 5 min, then 20 mL of the supernatant was mixed with 20 mL of water for analysis. Samples were analyzed by Xevo TQ-S triple quadrupole mass spectrometer. The ACQUITY UPLC BEH C18 (1.7 μm, 2.0 mm × 50 mm, Waters, USA) was used for the analysis. Gradient elution was applied consisting of 5 mM ammonium acetate aqueous solution containing 0.1% formic acid and acetonitrile containing 0.1% formic acid. After analyzing the concentrations of these compounds, the value of AUC_{last}, AUCINF_obs and MRTINF_obs was calculated from time-concentration curves in each animal using Phoenix WinNonlin (CERTARA, USA). C_{max} was determined as the maximum plasma concentration, and T_{max} was the time to reach the maximum concentration.

Statistical analysis

Data were presented as the mean ± SEM from at least three independent experiments. Comparisons between two or more groups were analyzed using two tailed unpaired Student's *t* test or one-way ANOVA. Statistical analyses were performed using GraphPad Prism software. Statistical significance was determined at $^{*}P < 0.05$; $^{**}P < 0.01$; $^{***}P < 0.001$.

RESULTS

DDRs are highly expressed in fibrotic lungs

To further demonstrate the potential links of DDRs with idiopathic pulmonary fibrosis (IPF) clinically, we measured its expression in the lung tissues from IPF patients. First, the pathological and normal tissue regions of IPF patient samples were investigated by H&E (Supplementary Fig. S1). The protein and mRNA levels of DDRs were much higher in IPF lung samples than normal control (Fig. 1a, b). The results of immunofluorescence also showed that DDR1/2 expression was much higher in PF lungs than that in the non-fibrosis part (Fig. 1c). These results indicated that DDRs shows high clinical correlation with idiopathic pulmonary fibrosis, indicating that DDRs may be a critical target for idiopathic pulmonary fibrosis.

Kinase inhibitory activity of XBLJ-13 and potential binding mode with DDRs

In our previous study, the indazole derivatives were found to be a series of potent DDRs inhibitors [16]. While these indazole derivatives lack selectivity and may associate with poor cell permeability issue. Based on the bio-isosterism strategy, we replaced the indazole scaffold with quinazoline scaffold to discover new DDRs inhibitors. Quinazoline scaffold in possession of biologically active nitrogen heterocyclic and a key pharmacore of ATP interacting with the hinge. Compound XBLJ-13 (Fig. 2a) was identified as one of the most potent agent in the series of quinazoline derivatives and was selected for further evaluation.

XBLJ-13 was tested for its DDRs kinase inhibitory properties using TR-FRET, exhibiting excellent inhibitory potencies against both DDR1 and DDR2 kinases with IC_{50} at 17.18 nM and 15.13 nM, respectively (Fig. 2b, c). Since DDRs show 61% homology with Abelson murine leukemia (Abl) kinase, most of the DDRs inhibitors are easy to target Abl undesirably. Despite of that, we surprisingly found that XBLJ-13 displayed a low inhibitory activity against Abl (Fig. 2d). To further evaluate the specificity, we carried out kinase profiling for XBLJ-13 against 34 kinases at the concentrations of 10, 100 nM, respectively. Results showed that 10 nM of XBLJ-13 hardly target other kinases except KDR with 60.8% inhibition. Comparably, XBLJ-13 possessed of relatively high selectivity with minimal inhibitory effect of PDGFR family and FGFR1 but showed strong inhibitory activity towards DDRs (Table 1).

To further characterize the potential binding mode of XBLJ-13 with DDRs protein, we conducted a molecular docking analysis using the Glide 4.0 module. And the predicted binding conformation was depicted in Fig. 2e, f. From the docking study, compound XBLJ-13 as a typical Type-II kinase inhibitor, adopted an extended conformation in the ATP binding site of DDR2, forming two essential hydrogen bonds with the residue Met657 at the hinge. The cyclopropyl-pyrazole group faced the solvent-accessible part and did not make any direct interaction with the protein. However, the other part of XBLJ-13, N-(3-(trifluoromethyl) phenyl) benzamide motif made further hydrogen bonding interactions with two residues Glu625 and Asp728 and the trifluoromethyl phenyl group located a hydrophobic subpacket near the α-Helix. Meanwhile compound XBLJ-13 was docked into the ATP binding site of DDR1 protein. Quinazolin-2-amine of compound XBLJ-13 formed two hydrogen bonds with the hinge residue Met657. This interaction pattern is similar to the bound

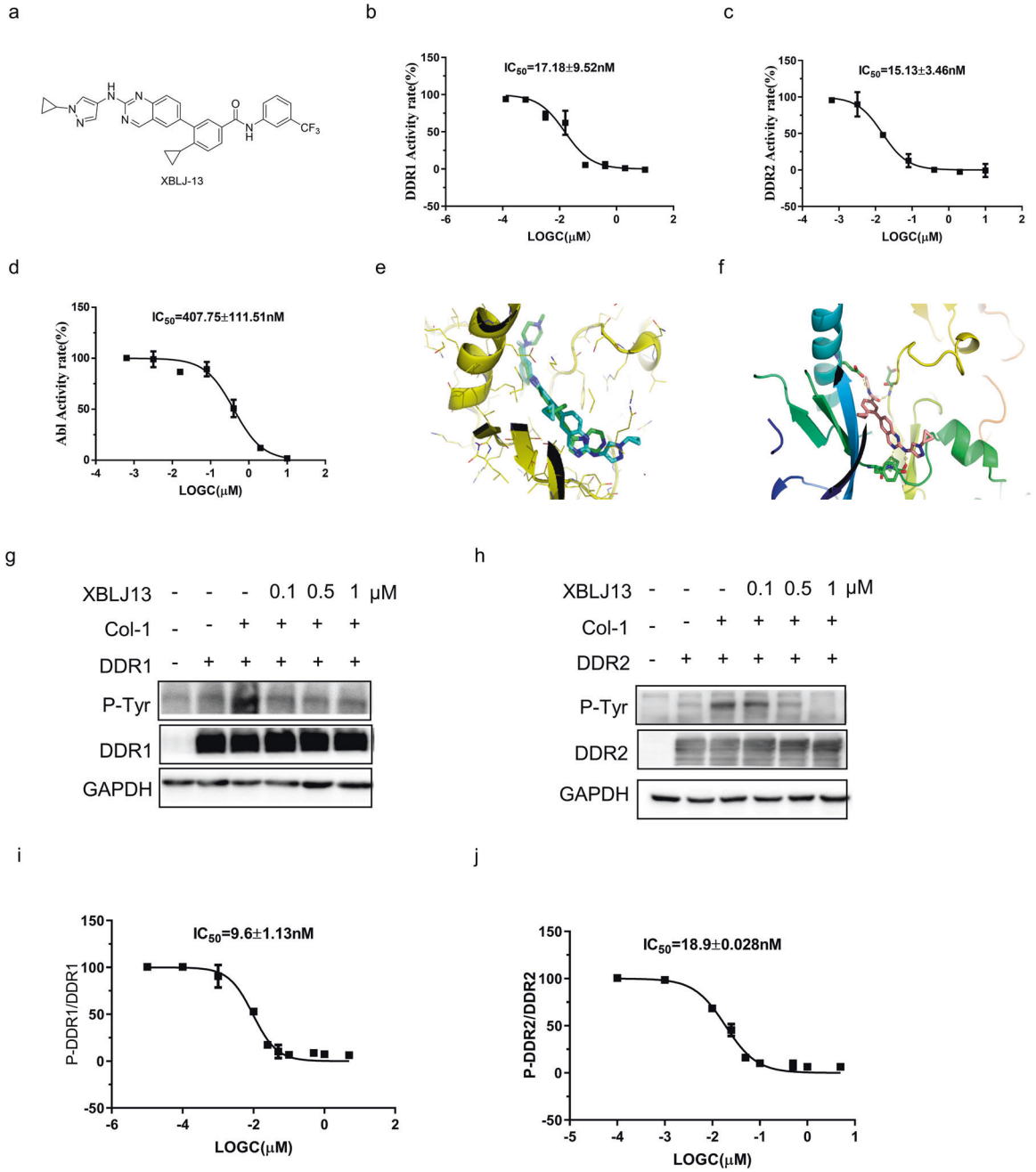

Fig. 2 The kinase inhibitory activity of XBLJ-13 and potential binding mode with DDRs. a The chemical structure of XBLJ-13. The inhibitory activity of XBLJ-13 on DDR1 (**b**) and DDR2 (**c**) kinases was tested in the LanthaScreen using 1:2 serial dilutions of the enzymes. XBLJ-13 was shown to inhibit both DDR1 and DDR2 activity with IC_{50} values of 17.18 nM for DDR1 and 15.13 nM for DDR2. Representative inhibition curves are shown. **d** Bcr-Abl activity experiments were performed using the HTRF KinEASE™ TK kit. XBLJ-13 was shown to inhibit Bcr-Abl activity with IC_{50} values of 407.75 nM. Experiments were performed using 30 μM ATP and representative inhibition curves are shown. **e** Molecular docking of XBLJ-13 into DDR1 (PDB: 6GWR). **f** Molecular docking of XBLJ-13 into the DDR2 homology model. **g**–**j** Overexpressed DDR1 or DDR2 HEK293T cells were treated with serial dilutions of XBLJ-13 then incubated with 10 μg/mL of collagen I. After 3 h, cells were lysed and the DDRs phosphorylation was determined by Western blot analysis (**g**, **h**) or by capture ELISA (**i**, **j**).

ligand from the crystal structure 6GWR, as indicated by the superimposition of two ligands. Also, similar to the docking study on DDR2, the trifluoromethyl-benzene group extended to alpha-Helix at the back side of the kinase catalytic domain.

XBLJ-13 inhibited collagen-induced auto-phosphorylation of DDRs
The high affinity of XBLJ-13 binding with DDRs kinase detected by the LanthaScreen Eu kinase binding assay (Table 1) suggested that XBLJ-13 would potently inhibit collagen-induced DDRs phosphorylation in cells. To analyze the DDRs-dependent cellular functional activity of XBLJ-13, HEK293T cells with or without DDRs overexpression were co-treated with collagen and XBLJ-13 or DMSO together for 2 h, followed by Western blot analysis with anti-phosphotyrosine (4G10) antibody to measure DDRs phosphorylation status. As shown in Fig. 2g, h, the increased DDRs tyrosine phosphorylation signal induced by collagen stimulation was

Table 1. Kinase inhibition by the XBLJ-13.

Kinase	100 nM	10 nM	Kinase	100 nM	10 nM
VEGFR-1	0.5	0	ALK	4.3	8.6
PDGFR-α	24.3	0	RET	−18.6	0.0
PDGFR-β	2.9	0	FGFR-1	58.2	37.1
C-Kit	39.3	25	KDR	100.	60.8
Flt-3	0	0	IR	37	13.4
EGFR	0	0	BTK	23.5	0.9
ErbB2	11.3	9.6	Tie2	3.1	1.3
ErbB4	75.7	25.1	CSF1R	12.9	4.6
Src	40.9	0	ITK	26.3	6
EPH-A2	83.5	30.2	FAK	18.6	19.3
IGF-1R	3.7	8.4	CDK4	6.6	2.2
AXL	11.4	17.5	CDK6	2.1	1.2
Met	−4.9	2.5	CDK1	6.5	3.2
MER	32.7	9.0	JAK1	0.6	0.5
ERK1	4.4	0.6	JAK2	3.0	1.1
ERK2	7.9	1.7	JAK3	2.5	2.6

inhibited by XBLJ-13 at 0.1–1 μM. To better determine the cellular IC_{50} values, we applied a capture ELISA assay to analyze the phosphorylated DDRs/total DDRs ratio which revealed the IC_{50} of XBLJ-13 was 9.6 nM against DDR1 phosphorylation, and the IC_{50} against DDR2 phosphorylation was 18.9 nM. XBLJ-13 with low IC_{50}s confirmed that it is a potent inhibitor of DDRs (Fig. 2i, j).

XBLJ-13 limits TGF-β-induced lung fibroblast to myofibroblast transition

With its excellent enzymatic specificity and inhibitory activity for DDRs, we further characterized the inhibition of the phenotypic fibroblast-to-myofibroblast transition by XBLJ-13, which represents one of the primary pathological mechanisms in fibrotic lung tissue. TGF-β1 was used to stimulate the fibroblast activation, which is a critical mediator of fibrogenic processes in PF. MRC-5 cells were treated with XBLJ-13 at the low concentration of 0.1, 0.5, 1 μM, which displayed non-toxic and had no effect on the proliferation rate of MRC-5 cells (Supplementary Fig. S1a). We confirmed that the DDRs kinase inhibitor XBLJ-13 can dose-dependently inhibit the activation of MRC-5 cells stimulated with TGF-β, which showed comparable effects as nintedanib (OFEV) in the protein and mRNA expression levels at 1 μM, characterized by almost 70% reduction of myofibroblast markers including fibronectin, collagen1-α1, and α-SMA (Fig. 3a–d). The similar anti-fibroblasts activation results were further obtained in primary mouse lung fibroblasts (Fig. 3e). As for TGF-β1-induced MRC-5 migration, XBLJ-13 significantly reduced migration ability (nearly 40%) of lung fibroblasts in wound-healing assay at 1 μM (Fig. 3f, g). In addition, XBLJ-13 restored the size of collagen gel lattices compared to TGF-β1 administered alone as demonstrated in the collagen gel contraction assay (Fig. 3h, i). Taken together, these data indicated that XBLJ-13 limited lung fibroblasts differentiation and activation induced by TGF-β.

XBLJ-13 inhibits DDRs related signaling pathways

To explore the underlying molecular mechanisms of XBLJ-13 towards lung fibroblasts activation, the phosphorylation levels of major downstream mediators of DDRs were analyzed. Compared with wild-type MRC-5, TGF-β treatment resulted in the phosphorylation of the downstream of DDRs kinase, including Akt/p38 and Erk/SRC pathway, while XBLJ-13 can significantly inhibit these signaling pathways with about 57%, 49%, 29 and 69% reduction rate separately at 1 μM (Fig. 4a–e). These results clearly revealed that XBLJ-13 might inhibit myofibroblasts activation through inhibiting the TGF-β-induced activation of DDRs signaling pathway.

XBLJ-13 demonstrates a good pharmacokinetic profile in vivo

Overall, considering the good activity in enzymatic assays and cellular anti-fibrosis assays, XBLJ-13 was subjected for in vivo pharmacokinetic assessment (CD-1 mice). XBLJ-13 (10 mg/kg) showed high exposure ($AUC_{(0-\infty)}$ 4467 ng·h/mL) and moderate C_{max} about 986 ng/mL, along with acceptable moderate half-life about 2.88 h. Nintedanib (BIBF1120) is a potent, oral, small-molecule tyrosine kinase inhibitor for treating IPF clinically. While nintedanib has unsatisfactory pharmacokinetic properties with $AUC_{(0-\infty)}$ of 2720 ng·h/mL and with $T_{1/2}$ of 5.15 h at 50 mg/kg oral administration in CD-1 mice. As we can see, XBLJ-13 displayed prominent pharmacokinetic properties with 4467 ng·h/mL $AUC_{(0-\infty)}$ at 10 mg/kg oral administration, strengthening our confidence of selecting XBLJ-13 as a lead compound. Table 2.

XBLJ-13 shows low cytotoxicity and hypo-toxicity in mice

Before exploring the ability of XBLJ-13 to combat lung fibrosis in vivo, we first evaluated its toxicity in both cellular and animal levels. First, we confirmed that XBLJ-13 showed no effect on cell viability in the lung fibroblasts cell line (MRC-5) and in the bronchial epithelium cell line (Beas-2B) for 72 h under the concentration of 10 μM (Supplementary Fig. S2a, 2b), whereas nintedanib showed obvious cell toxicity at the concentration of 5 μM. Further, the in vivo study of acute toxicity indicated that single administration of XBLJ-13 even at 500 mg/kg by oral route did not cause any lethality and no effects on general behaviors of mice. XBLJ-13 was observed to cause no significant change on the basic physiological properties of mice (e.g. blood glucose, body weight, respiratory rate and body temperature) after oral administration of 500 mg/kg compared to the control group injected with saline (Supplementary Fig. S2c-2f). Meanwhile, the effects of XBLJ-13 on biochemical parameters of experimental and control mice are detected and presented in Supplementary Fig. S1g, 1h. Oral administration of XBLJ-13 at 500 mg/kg did not cause significant differences on hepatic function indicators such as alanine amino transferase (ALT), aspartate amino transferase (AST), and lactate dehydrogenase (LDH). And kidney functional parameters such as creatinine (CRE), blood urea nitrogen (BUN), uric acid (UA) remained unchanged. Moreover, the hypo-toxicity of XBLJ-13 was confirmed with the histological HE stains of the liver, kidney, lung, spleen, and heart, which did not reveal any visible lesions or necrotic signs in all XBLJ-13 treated mice (Supplementary Fig. S2i). These data collectively showed that XBLJ-13 displayed a certain degree of drug safety for further pharmacological evaluation.

XBLJ-13 relieves bleomycin-induced lung injury and inflammation

Next, the therapeutic potential of compound XBLJ-13 on PF was substantiated in bleomycin-induced pulmonary fibrosis mice model in vivo, which is classic and widely used in IPF studies, with nintedanib as positive control. Histopathological evaluation of mice lung sections using H&E staining showed that BLM administration induced significant pulmonary damage, including the thickening of alveolar walls and accumulation of substantial inflammatory cells. Compound XBLJ-13 was orally administered at 30 or 60 or 90 mg/kg once daily (qd) for 12 days starting from the third day after bleomycin treatment. The lung injury induced by BLM was significantly attenuated by XBLJ-13 in the dose-dependent manners, which showed comparable inhibition ratio (32%) with nintedanib at the concentration of 60 mg/kg (Fig. 5a, b). BLM administration significantly up-regulated the total cell number and protein concentration in bronchoalveolar Lavage Fluid (BALF), while XBLJ-13 could significantly attenuate those almost by half at the same concentration with nintedanib (Fig. 5c, d). In the serum level, XBLJ-13 effectively inhibited ALP

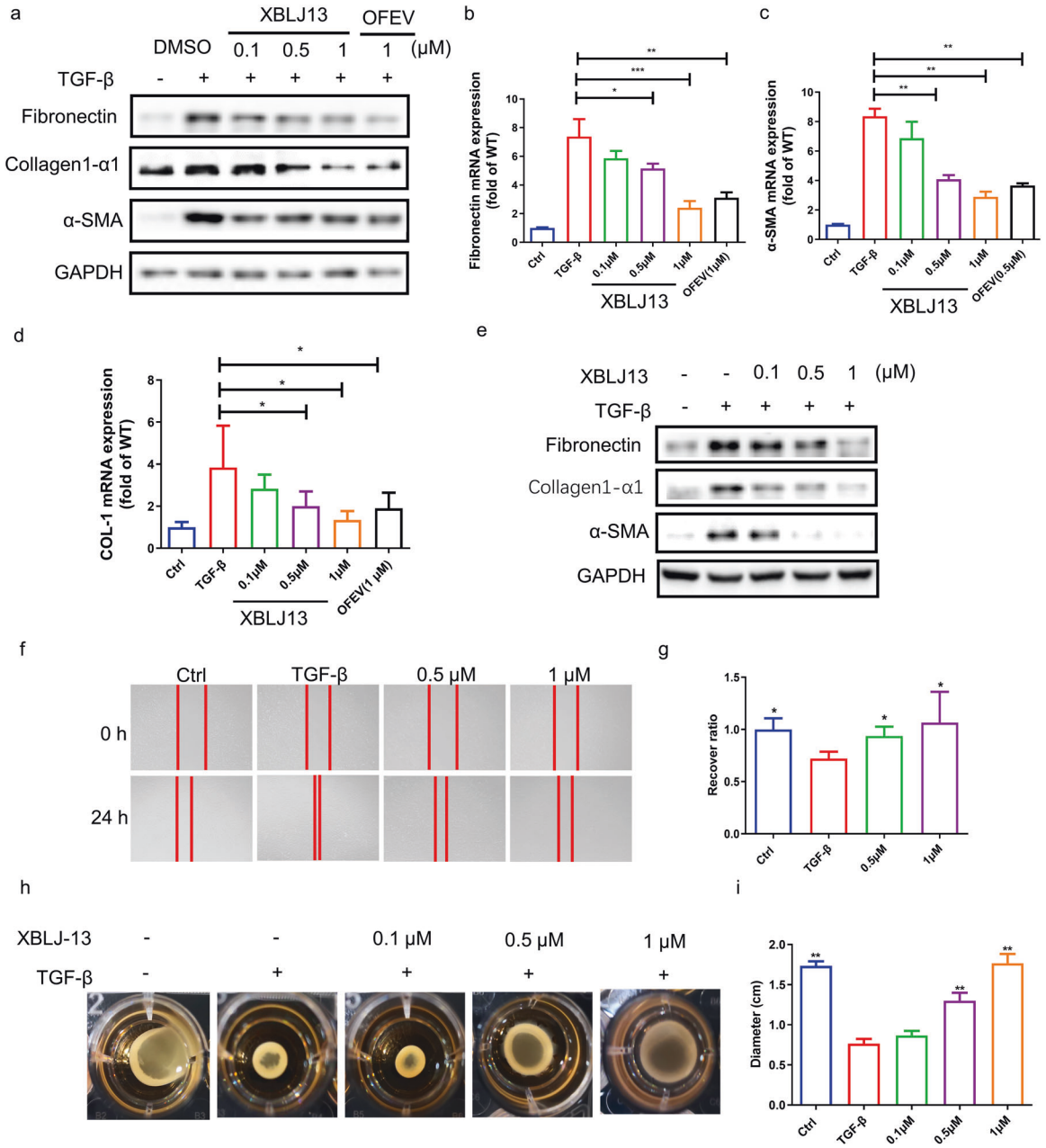

Fig. 3 XBLJ-13 limits TGF-β-induced lung fibroblast to myofibroblast transition. (**a**) Confluent MRC-5 cells were stimulated with TGF-β (5 ng/mL) and treated with different concentrations of XBLJ-13 for 24 h. Representative Western blots were shown. (**b**–**d**) Confluent MRC5 were stimulated with TGF-β (5 ng/mL) and treated with different concentrations of XBLJ-13 for 24 h. Representative mRNA levels of Fibronectin, α-SMA, and COL-1 were shown. (**e**) Confluent primary lung fibroblasts were stimulated with TGF-β (5 ng/mL) and treated with different concentrations of XBLJ-13 for 24 h. Representative Western blots were shown. (**f**, **g**) Wound healing assays of MRC-5 stimulated with TGF-β (5 ng/mL) and treated with different concentrations of XBLJ-13 for 48 h. The mobility rate histograms of each group were shown. (**h**, **i**) MRC-5 cells were seeded in the collagen gel with or without TGF-β (5 ng/mL) and XBLJ-13 (0.1, 0.5, and 1 μM) for 2 days, and then the areas of the collagen gel were measured for analysis. The statistical significance was compared with the TGF-β group with one-way ANOVA followed by Dunnett's multiple comparisons. *$P < 0.05$, **$P < 0.01$, ***$P < 0.001$.

concentration from 159.28 ± 36.72 U/L to 97.53 ± 27.56 U/L and LDH concentration from 1183.29 ± 324.35 U/L to 832.12 ± 187.57 U/L, which are important markers of lung injury (Fig. 5e, f). However, nintedanib only showed minimal effect on these injury markers. Then the mRNA levels of pro-inflammatory cytokines in lung tissues were also examined using RT-qPCR. BLM instillation significantly increased the level of TNF-α (7.6-fold), IL-1β (4.4-fold) and IL-6 (6.9-fold) in the lung tissues compared with the control group, which were diminished by compound XBLJ-13 treatment dose dependently (Fig. 5g–i). The immunohistochemical staining of F4/80 of the lung tissues also showed that XBLJ-13 significantly attenuated lung macrophage infiltration (Fig. 5j), which was consistent with the cellular results that XBLJ-13 inhibited the mRNA expression of M1-like polarization markers including TNF-α, MCP-1, iNOS and IL-6 induced by LPS in macrophages (Supplementary Fig. S3a–d). These data implied that XBLJ-13 has the direct anti-inflammation effect. Collectively, administration of XBLJ-13 alleviated BLM induced lung injury and inflammatory responses, displaying comparable effects with nintedanib or even better.

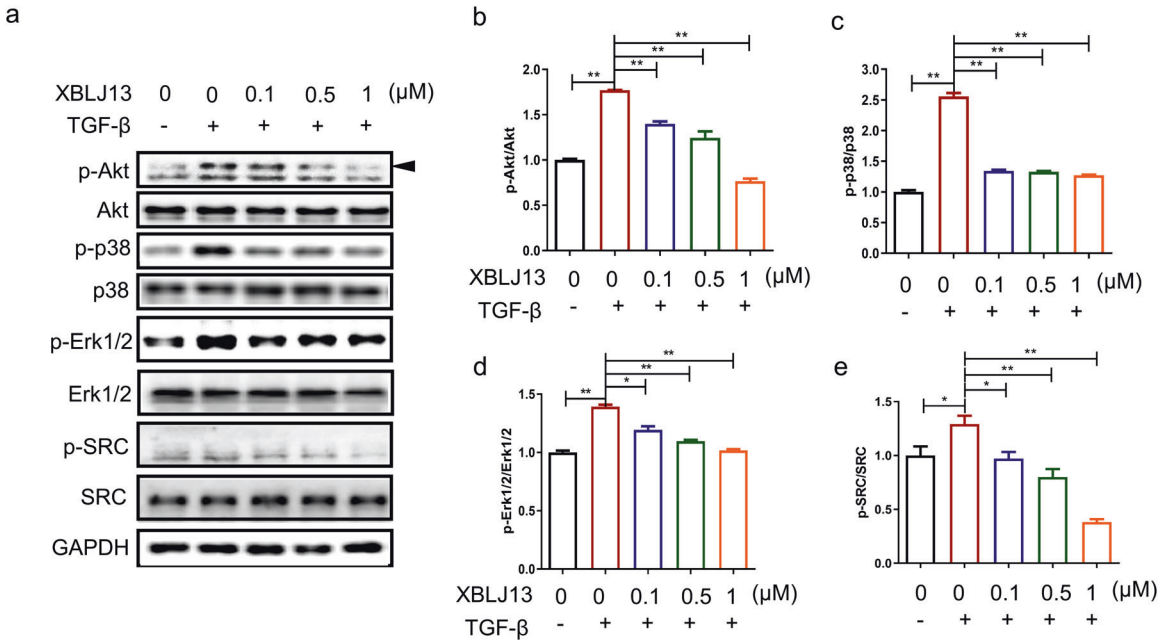

Fig. 4 XBLJ-13 inhibits DDRs associated signaling pathways. a MRC5 were incubated with TGF-β1 (5 ng/mL) and treated with different concentrations of XBLJ-13 for 24 h. p-AKT, AKT, p-P38, p38, p-ERK, ERK, p-SRC, SRC expression were analyzed by Western blotting. **b**–**e** Quantitative analysis showed the fold change of these phosphorylation levels in (**a**). The statistical significance was compared with the TGF-β group with one-way ANOVA followed by Dunnett's multiple comparisons. *$P < 0.05$, **$P < 0.01$.

Table 2. Plasma-derived PK parameters of the XBLJ-13 and nintedanib.

Property	XBLJ-13	Nintedanib
Concentration (mg/kg)	10	50
MRT_{INF_obs} (h)	4.42 ± 0.57	5.19
AUC_{INF_obs} (h·ng/mL)	4467 ± 516	2720
AUC_{last} (h·ng/mL)	4451 ± 522	NA
C_{max} (ng/mL)	986 ± 161	547
T_{max} (h)	2.00 ± 00	N/A
$T_{1/2}$ (h)	2.88 ± 0.32	5.15

[a]Formulation: DMAC/0.5% methylcellulose (5:95, *v/v*); AUC = area under the curve; C_{max} = maximal concentration; MRT = mean residence time; NA = not applicable; $T_{1/2}$ = half-life; only representative PK data are listed here. Linear dose dependency and no sex effect was observed.

XBLJ-13 attenuates bleomycin-induced pulmonary fibrosis

Based on these anti-inflammation results of XBLJ-13, we further investigated its efficacy on lung fibrosis induced by bleomycin in vivo. Masson's Trichome staining demonstrated that XBLJ-13 ameliorated the collagen deposition induced by BLM in a dose-dependent manner. The consistent results were validated in immunohistochemistry (IHC) analysis, exhibiting a downregulated α-SMA expression in XBLJ-13 treated groups (Fig. 6a, b). Primary lung fibroblasts separated from XBLJ-13 treated mouse showed lower Collagen1-1 and fibronectin expression than bleomycin treated group (Supplementary Fig. S4). Hydroxyproline, the main component of collagen, was similarly significantly inhibited by 29% under 60 mg/kg XBLJ-13 treatment compared with vehicle group, while nintedanib showed no significance (Fig. 6c). Since TGF-β1 is considered as an important master switch for the induction of fibrotic progression during PF, we investigated the inhibitory effect of XBLJ-13 on TGF-β1 in BALF. As we can see from Fig. 5d, XBLJ-13 (90 mg/kg) suppressed the active TGF-β1 from 123 pg/mL to 48 pg/mL. The transcription levels of fibrosis-related markers in lung tissues were also examined by RT-qPCR. XBLJ-13 (60 and 90 mg/kg) treatment significantly decreased the expression of TGF-β1, collagen1-α1 and α-SMA by about 90% (Fig. 6e–g). Therefore, the administration of XBLJ-13 significantly attenuated BLM induced pulmonary fibrosis, displaying similar effects with nintedanib or even better.

DISCUSSION

IPF is a devastating and grievous disease for which the only beneficial treatment modality is lung transplantation. Although a number of potential therapeutic targets are being investigated, no approved course of treatment currently exists that halts the progression of IPF and prolongs survival effectively [17]. Therefore, the identification of novel therapeutic strategies for treating IPF is a large unmet medical need. Recently, some compelling findings shed new light on this therapeutic area and identified DDRs as a novel and potential target in IPF. Their unique ligands (collagens) of DDRs and its prolonged active mechanism implied a different strategy for the treatment of IPF [18]. The collagen is an important extracellular matrix component that directs many fundamental cellular processes including differentiation, proliferation, and motility. Collagen-1-DDRs pathway is frequently upregulated and plays critical roles in idiopathic pulmonary fibrosis formation and progression [19]. Therefore, the inhibition of increased DDRs signaling could have a significant potential in the treatment of idiopathic pulmonary fibrosis in which the DDRs pathway is aberrantly activated.

In this study, we assessed the anti-fibrosis efficacy of XBLJ-13, an orally bioavailable small molecule selectively targeting the catalytic activity of DDRs kinase. XBLJ-13 potently inhibited DDRs phosphorylation and the activation of its key downstream effectors in lung fibroblast cell lines. Correspondingly, XBLJ-13 potently inhibited TGF-β mediated activation of lung fibroblasts. Prior to initiating XBLJ-13 in vivo efficacy studies, we analyzed the toxicology and pharmacokinetic characters of XBLJ-13 which showed higher oral bioavailability and greater safety than nintedanib. More importantly, the oral dosing of XBLJ-13 resulted in a marked anti-inflammation and anti-fibrosis activity in the bleomycin induced lung fibrosis model.

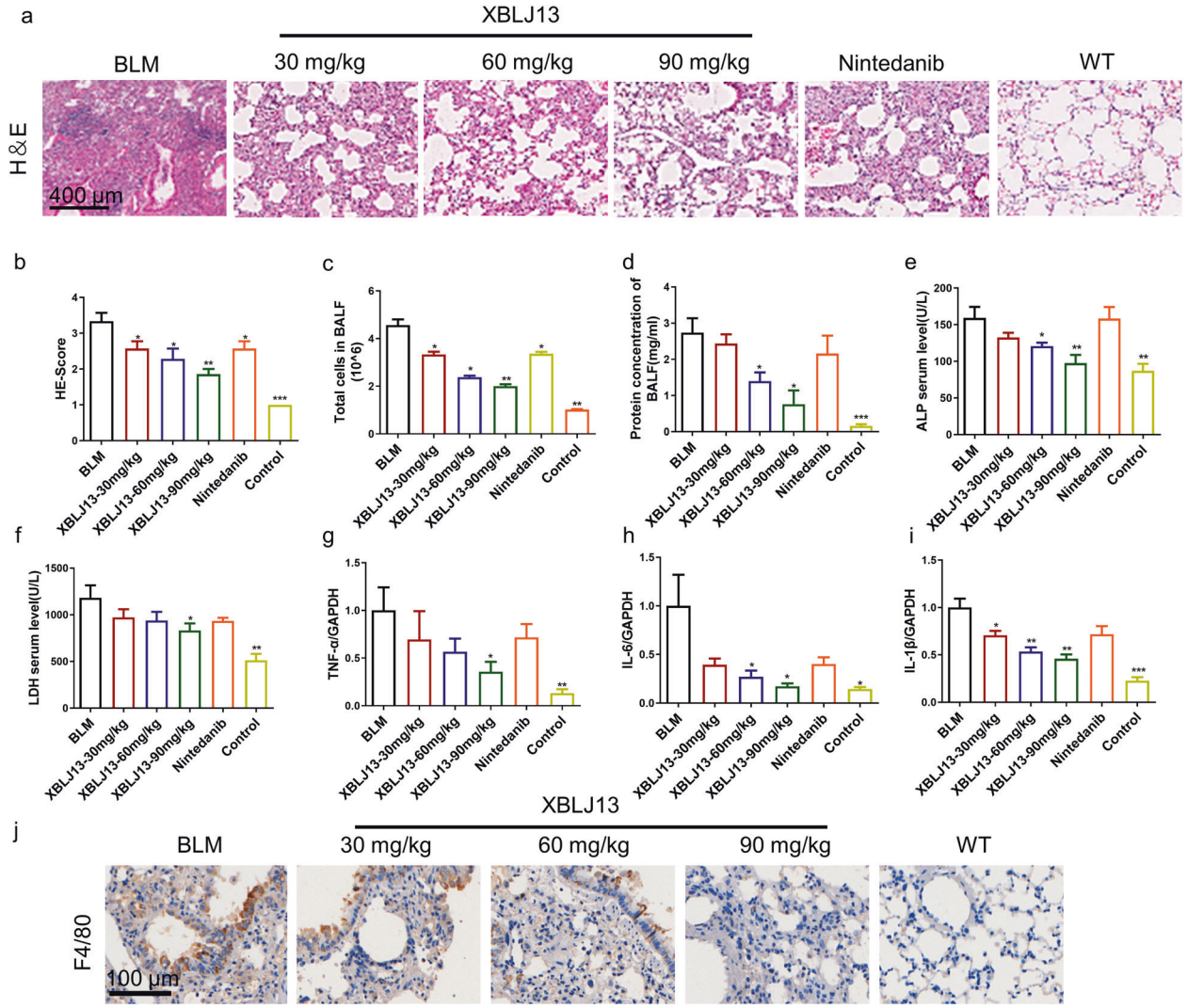

Fig. 5 Effect of XBLJ-13 on BLM induced lung inflammation and lung injury. Mice were intratracheally instilled with BLM (1.7 U/kg) or with vehicle only. The indicated dose (mg/kg) of XBLJ13 and nintedanib were given once daily for 12 days ($n = 8$ per group). **a** Sections of lung tissue were prepared on day 15 after BLM treatment and subjected to H&E staining. **b** The score of H&E stains. **c** The total cell number and (**d**) the protein concentration in BALF. **e**, **f** The ALP and LDH serum level. **g**–**i** The mRNA levels of various inflammatory factors, including TNF-α, IL-6 and IL-1β were determined as described in the methods. **j** Immunohistochemical staining of F4/80 of the lung tissues. Results are presented as mean ± SEM. The statistical significance was compared with the BLM group with one-way ANOVA followed by Dunnett's multiple comparisons. $^{*}P < 0.05$, $^{**}P < 0.01$, $^{***}P < 0.001$.

An interesting feature of XBLJ-13 is its selectivity against DDRs. XBLJ-13 presented IC_{50} values for DDRs in the nanomolar range in a kinase assay and showed at least more than 100-fold selectivity over a panel of tyrosine kinases including VEGFR1, PDGFR-α, PDGFR-β, and SRC. Even though, XBLJ-13 showed the same or even better anti-fibrosis activity in vivo and in vitro than nintedanib with low kinase selectivity, indicating the potent effect of targeting DDRs. It is worth noting that most of the reported DDRs kinase inhibitors being clinically evaluated are not very specific for DDRs and exhibit activities against multiple kinases, often resulting in unwanted off-target toxicity [20]. By lacking the confounding issue of off-target kinase inhibition, XBLJ-13 might overcome the forementioned limitations of other DDRs inhibitors and could specifically achieve the therapeutic potential of DDRs inhibition.

Previous studies have shown that the knockout of DDR1 or DDR2 both showed a similar phenotype that resisted pulmonary fibrosis [7, 10], but which DDRs subtype plays a more important role in pulmonary fibrosis is still unknown. Therefore, it is still necessary to discover DDR1 or DDR2 inhibitors with high selectivity to explore the specific roles of DDR1 and DDR2 in pulmonary fibrosis. Even though XBLJ-13 is not selective for DDR1/2, it may provide a new framework structure for the optimization of selective inhibitors of DDR1/2.

ACKNOWLEDGEMENTS

This study was supported by National Natural Science Foundation of China (No. 81773779, 81125023, U1703235, 31871414, and 81701220), Shanghai Science and Technology Development Funds (19JC1416300 and 18431907100), Key New Drug Creation and Manufacturing Program of China (2019ZX09201001–004–010, 2019ZX09201001–003–010, and 2018ZX09711002–004–009), Shanghai Aging and Maternal and Child Health Research Program (2020yjzx0136), Backbone Program of Shanghai Pulmonary Hospital (fkgg1809) and K. C. Wong Education Foundation.

AUTHOR CONTRIBUTIONS

YD and BXT contributed equally, and they performed biological experiments and drafted the manuscript. DQC, QW and LWZ performed the chemical synthesis. CL

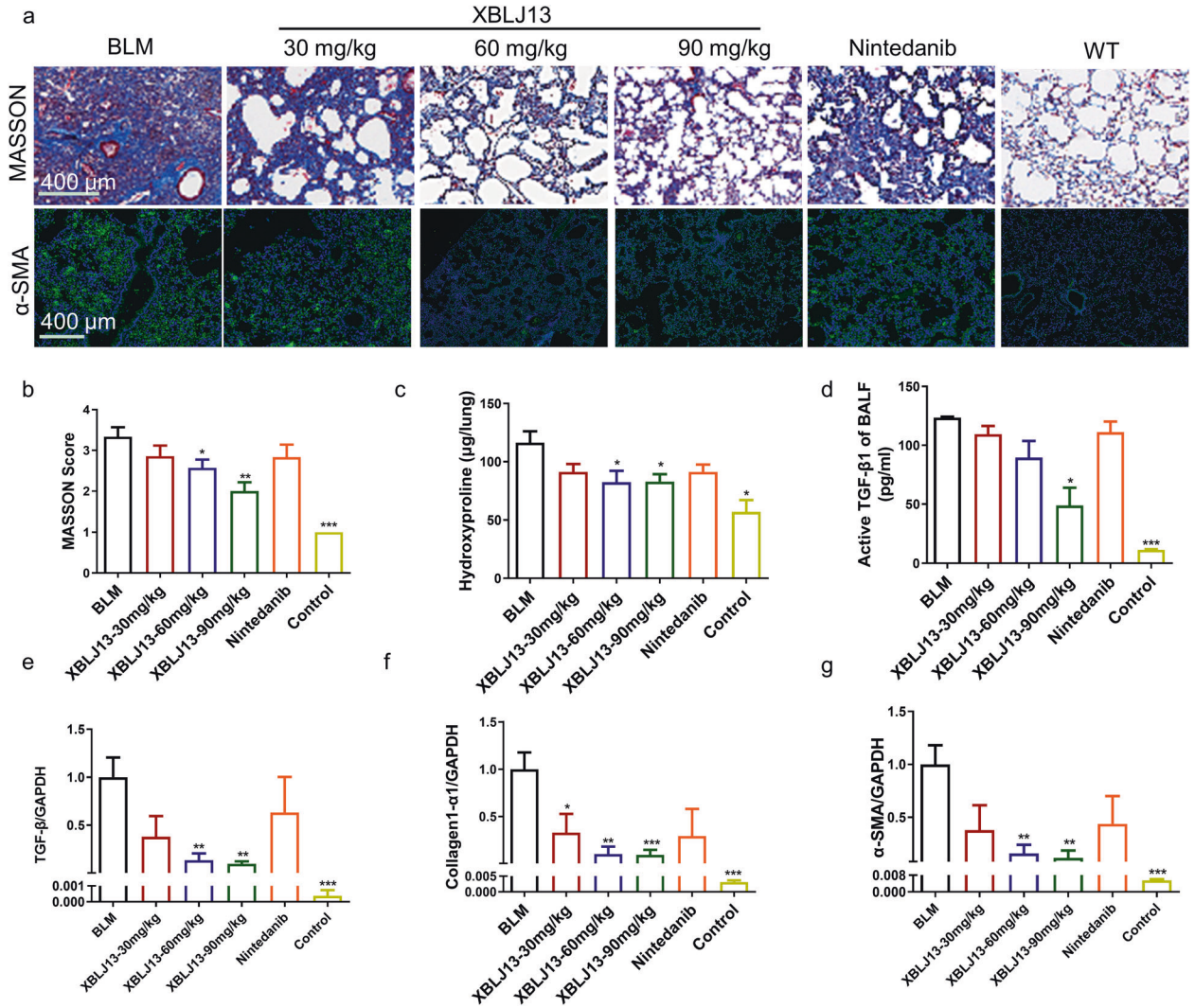

Fig. 6 Effect of XBLJ-13 on BLM induced lung fibrosis. Mice were intratracheally instilled with BLM (1.7 U/kg) or with vehicle only. The indicated dose (mg/kg) of XBLJ13 and nintedanib were given once daily for 12 days ($n = 8$ per group). **a** Sections of lung tissue were prepared on day 15 after BLM treatment and subjected to MASSON staining and immunofluorescence staining of α-SMA. **b** The score of MASSON staining. **c** Hydroxyproline of the whole lung. **d** The active TGF-β1 level in BALF evaluated by ELISA. **e**–**g** The mRNA levels of various fibrosis associated markers, including TGF-β1, collagen1-α1, and α-SMA, were determined as described in the Methods. Results are presented as mean ± SEM. The statistical significance was compared with the BLM group with one-way ANOVA followed by Dunnett's multiple comparisons. $^{*}P < 0.05$, $^{**}P < 0.01$, $^{***}P < 0.001$.

performed the kinome selectivity assay. XZ, DDS and XS helped with the animal experiments. HS provided the human lung tissues. YZ, DQC, BX, XMZ and JL corrected the manuscript and directed the study. All authors have given approval to the final version of the manuscript.

ADDITIONAL INFORMATION

Supplementary information The online version contains supplementary material available at https://doi.org/10.1038/s41401-021-00808-z.

Competing interests: The authors declare no competing interests.

REFERENCES

1. Zank DC, Bueno M, Mora AL, Rojas M. Idiopathic pulmonary fibrosis: aging, mitochondrial dysfunction, and cellular bioenergetics. Front Med. 2018;5:10.
2. Richeldi L, Collard HR, Jones MG. Idiopathic pulmonary fibrosis. Lancet. 2017;389:1941–52.
3. Glass DS, Grossfeld D, Renna HA, Agarwala P, Spiegler P, Kasselman LJ, et al. Idiopathic pulmonary fibrosis: Molecular mechanisms and potential treatment approaches. Respir Investig. 2020;58:320–35.
4. Wynn TA. Integrating mechanisms of pulmonary fibrosis. J Exp Med. 2011;208:1339–50.
5. Byrne AJ, Maher TM, Lloyd CM. Pulmonary macrophages: a new therapeutic pathway in fibrosing lung disease? Trends Mol Med. 2016;22:303–16.
6. Grimminger F, Günther A, Vancheri C. The role of tyrosine kinases in the pathogenesis of idiopathic pulmonary fibrosis. Eur Respir J. 2015;45:1426–33.
7. Avivi-Green C, Singal M, Vogel WF. Discoidin domain receptor 1-deficient mice are resistant to bleomycin-induced lung fibrosis. Am J respiratory Crit Care Med. 2006;174:420–7.
8. Flamant M, Placier S, Rodenas A, Curat CA, Vogel WF, Chatziantoniou C, et al. Discoidin domain receptor 1 null mice are protected against hypertension-induced renal disease. J Am Soc Nephrol. 2006;17:3374–81.
9. Matsuyama W, Wang L, Farrar WL, Faure M, Yoshimura T. Activation of discoidin domain receptor 1 isoform b with collagen up-regulates chemokine production in human macrophages: role of p38 mitogen-activated protein kinase and NF-kappa B. J Immunol (Baltim, Md: 1950). 2004;172:2332–40.
10. Zhao H, Bian H, Bu X, Zhang S, Zhang P, Yu J, et al. Targeting of discoidin domain receptor 2 (DDR2) prevents myofibroblast activation and neovessel formation during pulmonary fibrosis. Mol Ther. 2016;24:1734–44.
11. Poudel B, Yoon DS, Lee JH, Lee YM, Kim DK. Collagen I enhances functional activities of human monocyte-derived dendritic cells via discoidin domain receptor 2. Cell Immunol. 2012;278:95–102.

12. Ruiz PA, Jarai G. Collagen I induces discoidin domain receptor (DDR) 1 expression through DDR2 and a JAK2-ERK1/2-mediated mechanism in primary human lung fibroblasts. J Biol Chem. 2011;286:12912–23.
13. Day E, Waters B, Spiegel K, Alnadaf T, Manley PW, Buchdunger E, et al. Inhibition of collagen-induced discoidin domain receptor 1 and 2 activation by imatinib, nilotinib and dasatinib. Eur J Pharmacol. 2008;599:44–53.
14. Jeffries DE, Borza CM, Blobaum AL, Pozzi A, Lindsley CW. Discovery of VU6015929: a selective discoidin domain receptor 1/2 (DDR1/2) Inhibitor to explore the role of DDR1 in antifibrotic therapy. ACS medicinal Chem Lett. 2020;11:29–33.
15. Ngo P, Ramalingam P, Phillips JA, Furuta GT. Collagen gel contraction assay. Methods Mol Biol. 2006;341:103–9.
16. Wang Q, Dai Y, Ji Y, Shi H, Guo Z, Chen D, et al. Discovery and optimization of a series of 3-substituted indazole derivatives as multi-target kinase inhibitors for the treatment of lung squamous cell carcinoma. Eur J Med Chem. 2019;163:671–89.
17. Richeldi L, Varone F, Bergna M, de Andrade J, Falk J, Hallowell R, et al. Pharmacological management of progressive-fibrosing interstitial lung diseases: a review of the current evidence. Eur Respir Rev. 2018;150:21–7.
18. Moll S, Desmouliere A, Moeller MJ, Pache JC, Badi L, Arcadu F, et al. DDR1 role in fibrosis and its pharmacological targeting. Biochim Biophys Acta Mol Cell Res. 2019;1866:118474.
19. Borza CM, Pozzi A, Plosa EJ. Discoidin domain receptor 2, a potential therapeutic target in lung fibrosis. Am J Respir Cell Mol Biol. 2018;59:277–8.
20. Guignabert C, Phan C, Seferian A, Huertas A, Tu L, Thuillet R, et al. Dasatinib induces lung vascular toxicity and predisposes to pulmonary hypertension. J Clin Invest. 2016;126:3207–18.